American Journal of Pathology, Vol. 165, No. 5, November 2004

Molecular Pathogenesis of Genetic and Inherited Diseases

Biliary Dysgenesis in the PCK Rat, an Orthologous Model of Autosomal Recessive Polycystic Kidney Disease

Tatyana V. Masyuk,* Bing Q. Huang,* Anatoliy I. Masyuk,* Erik L. Ritman,† Vicente E. Torres,‡ Xiaofang Wang,‡ Peter C. Harris,‡ and Nicholas F. LaRusso*

From the Divisions of Gastroenterology and Hepatology and Nephrology‡ and the Department of Physiology and Bioengineering,† Mayo Clinic, Rochester, Minnesota*

Hepatic polycystic disease occurs alone or in combination with polycystic kidney disease (PKD). In autosomal recessive PKD (ARPKD), liver lesions are the major cause of morbidity and mortality in older patients. ARPKD is caused by a mutation to *PKHD1* and the PCK rat is an orthologous model of disease. Recently, we showed that fibrocystin, *Pkhd1* protein, is localized to primary cilia in rat cholangiocytes and that disruption of its ciliary expression results in biliary cystogenesis. This study describes biliary phenotype in the PCK rat using micro-computed tomography scanning and three-dimensional reconstruction, and light, scanning, and transmission microscopy. Our results show that the biliary tree undergoes extensive remodeling resulting in bile duct dilatation, focal budding, and formation of cysts that are initially connected to bile ducts, but throughout time separate from them. Progressive liver enlargement results from massive cyst formation while liver parenchymal volume remains unchanged. Cilia in cystic cells are abnormal consistent with the notion that the primary defect in ARPKD resulting in cystogenesis may be linked to ciliary dysfunction. Our results suggest that the PCK rat is a useful model for studies of biliary cystogenesis and treatment options of inherited cystic liver disease. *(Am J Pathol 2004, 165:1719–1730)*

Hepatic polycystic disease occurs alone[1–4] or in combination with polycystic kidney disease (PKD).[5–8] PKD is a multiorgan genetic disease and can be inherited as autosomal dominant (ADPKD) or autosomal recessive (ARPKD). In ARPKD, ~30% of affected neonates die because of greatly enlarged kidneys detected *in utero* or in the perinatal period. In surviving ARPKD patients, hepatic lesions become progressively more severe with age and liver disease is a major cause of morbidity and mortality. Biliary dysgenesis is characterized by congenital hepatic fibrosis, intrahepatic bile duct dilatation (Caroli's disease), and/or cyst development.[6,7]

Several mouse and rat models of recessive PKD have been described,[9–12] each varying by age of disease onset, affected portion of renal tissue, or hepatic involvement. Many of the genes causing these disorders have been identified and characterized but none correspond to the human ARPKD gene.[13–16] Animal models generated by chemical mutagenesis also exist.[9,12,15–18] In some of these models, only the kidneys are affected, in others in addition to renal disease, hepatic abnormalities have been described.[12,14,16–20]

In 2000 a new rat model, the PCK rat, derived from a colony of Crj:CD (SD) was reported.[21] Sanzen and colleagues[22] described that the liver pathology in the PCK rats up to 4 months of age was characterized by progressive liver enlargement and multiple saccular and segmental dilatations of the intrahepatic bile ducts. In a parallel study, Lager and colleagues[23] evaluated renal and hepatic lesions in PCK rats up to 182 days of age. It was recently shown that the PCK rat has a spontaneous splicing mutation IVS35–2A→ T.[24] Linkage and gene cloning analysis confirmed that kidney and liver disease in ARPKD patients and in PCK rats is caused by mutations to orthologous genes, *PKHD1/Pkhd1.* The product of *PKHD1*, fibrocystin, is a novel protein with unknown function.[25,26] Recently, we[27,28] and others[29–36] have shown that PKD-related proteins, including fibrocystin, are localized to primary cilia in liver and kidney and that

Supported by the National Institutes of Health (grants DK24031 to N.F.L., DK44863 to V.E.T., DK59597 to P.C.H., and EB000305 to E.L.R.), the Polycystic Kidney Disease Foundation (postdoctoral fellowship to T.V.M.), and the Mayo Foundation.

Accepted for publication July 27, 2004.

Address reprint requests to Nicholas F. LaRusso, M.D., Mayo Medical School, Clinic and Foundation, 200 First St., SW, Rochester, MN 55905. E-mail: larusso.nicholas@mayo.edu.

disruption of their ciliary expression (either by a germ line mutation or experimentally induced) results in kidney and biliary cystogenesis.

It is well known that, in ADPKD, the majority of renal[5] and liver[37] cysts are disconnected from the kidney tubules and biliary ducts, respectively, as they grow. However, to our knowledge, the fate of cysts in the liver as well as in the kidney in ARPKD is unknown. Sanzen and colleagues[22] concluded based on their data that, in the PCK rat by the age of 4 months, cystic changes of the liver were found not to be true cysts but multiple segmental and cystic dilatations of the intrahepatic bile ducts.

In this study, to further characterize biliary dysgenesis in the PCK rat, especially the question of whether liver cysts disconnect from the biliary tree during disease progression, we investigated: 1) the effect of *Pkhd1* mutation on intrahepatic biliary tree remodeling throughout the course of disease progression; 2) the effect of cyst formation on hepatic parenchymal and biliary tree volumes; 3) morphological alterations associated with progressive growth of the intrahepatic biliary tree and cyst formation; and 4) ciliary morphology in cystic epithelia in two groups of PCK rats (3 and 6 month old).

Materials and Methods

Animals and Experimental Models

All studies were performed after approval of the Mayo Institutional Animal Care and Use Committee. We used 3-month-old ($n = 18$) and 6-month-old ($n = 9$) normal rats and 3-month-old ($n = 22$) and 6-month-old ($n = 24$) PCK rats. Based on our data and previously published observations[38,39] that liver morphology and liver weight-to-body weight ratios remain unchanged in normal rats up to 24 months of age, in most of the experiments only one group (3 months old) of normal rats was used as controls. Given the fact that liver weight is increased with age in normal rats, in some experiments, 6-month-old normal rats were used.

Three-Dimensional Reconstruction of the Intrahepatic Biliary Tree

The biliary trees of normal and PCK rats were reconstructed in three-dimensions using a technique previously published by us.[40] Briefly, rats were anesthetized with pentobarbital (50 mg/kg body wt, i.p.) and a low-viscosity, lead chromate-containing radiopaque liquid silicone polymer (MV-122; Flow Tech, Inc., Carver, MA) was injected retrogradely through the common bile duct. Each liver lobe was fixed in 10% buffered formalin, transferred to a solution of glycerin in water with increasing concentrations from 30 to 100%, suspended in a thin-walled plastic cylinder, and clear BioPlastic polymer poured around for setting into a hard cylinder. Specimens were scanned using a micro-computed tomography (CT) scanner, which consists of a spectroscopic X-ray source, a fluorescent crystal plate, a lens, and a charge-coupled device (CCD) detector array. Our micro-CT scanner uses a Philips spectroscopy X-ray tube with 12 mm $\times$ 0.4 mm line-focus focal spot. The specimen was mounted on a stack of computer-controlled precision stages: 1) an inclination stage that is used to position a specimens' rotation axis at right angles to the X-ray beam; 2) a linear translation stage with 0.1 μm resolution and 1.4 μm repeatability; 3) a rotation stage with 0.01° step size, 0.01° accuracy, and 0.001° resolution; and 4) a Huber goniometer stage that allows the specimen to be placed in a symmetrical (or if desired, asymmetrical) position about the axis of rotation. The specimen was positioned close to the crystal plate and rotated in 721 equiangular steps around 360° between each X-ray exposure and its accompanying CCD recording. The transmitted X-rays were converted to visible light by a fluorescent crystal plate. The light image generated within the crystal plate was transferred by the lens of a microscope objective onto the surface of a CCD camera. The charge of each pixel was digitized and stored as an array in a computer until all projections, at small increments of specimen rotation around 360°, had been acquired. The focus, rotation, and translation stages were controlled with a computer.

Specimens were scanned at resolution of 20 μm and a modified Feldkamp cone beam backprojection algorithm was applied to generate three-dimensional images. To visualize bile ducts with diameters less than 20 μm, small distal (close to the edge) pieces of the liver lobe of normal and 3-month-old PCK rats were reconstructed with resolution of 5 μm. Quantitative analysis was performed using Analyze (Biomedical Imaging Resource; Mayo Foundation, Rochester, MN). The diameters of proximal and distal bile duct segments, the number of interbranch segments (ie, the part of the biliary tree between two bifurcations), the length of interbranch segments, the length of the biliary tree, and the total biliary tree volume were quantified as previously described.[40]

To visualize liver parenchyma and liver cysts, intact livers (without injection of contrast agent) were prepared, scanned, and reconstructed as described above. We could distinguish liver parenchyma and fluid-filled cysts based on differences in density. Volumes of whole liver and cysts were measured from each scanned slice (up to 800 slices were used) and total volumes calculated as the sum. Parenchymal volume was calculated as the difference between total liver and total cystic volume.

Microdissection of the Liver Cysts

PCK rats were anesthetized with pentobarbital (50 mg/kg body wt, i.p.), the portal vein cannulated using PE-50 tubing, and blood flushed out with 0.9% sodium chloride. The liver was removed, placed in cold buffer containing 115 mmol/L NaCl, 5 mmol/L KCl, 0.8 mmol/L KH_2PO_4, 25 mmol/L Hepes, 2 mmol/L $CaCl_2$, 0.8 mmol/L $MgSO_4$, 2.5 mmol/L glucose, pH 7.4. Liver cysts were microdissected under a dissecting scope and, using higher magnification, residual hepatocytes and connective tissue were removed.

Immunochistochemistry

The liver was perfusion-fixed with 4% paraformaldehyde/2% glutaraldehyde in 0.1 mol/L phosphate-buffered

saline, paraffin-embedded, and sectioned at 4-μm-thick sections. Sections were stained with hematoxylin and eosin (H&E); CK-19 (diluted 1:50; Sigma, St. Louis, MO); and Masson's trichrome.

Transmission and Scanning Electron Microscopy

For transmission and scanning electron microscopy liver first was perfused with 4% paraformaldehyde/2% glutaraldehyde in 0.1 mol/L phosphate-buffered saline. Transmission electron microscopy of liver tissue after fixation in 4% paraformaldehyde/2% glutaraldehyde for 2 hours was performed with a Joel 1200 electron and scanning electron microscopy with Hitachi S-4700 microscopes. For transmission electron microscopy, samples were postfixed in 1% osmium tetroxide for 1 hour, rinsed in distilled water, dehydrated, embedded in Spurs resin, and sectioned at 80 nm. Samples for scanning electron microscopy were incubated in 1% osmium tetroxide for 30 minutes, dehydrated, dried in a critical point drying device, mounted onto specimen stubs, and sputter coated with gold-palladium alloy. Scanning electron mi-

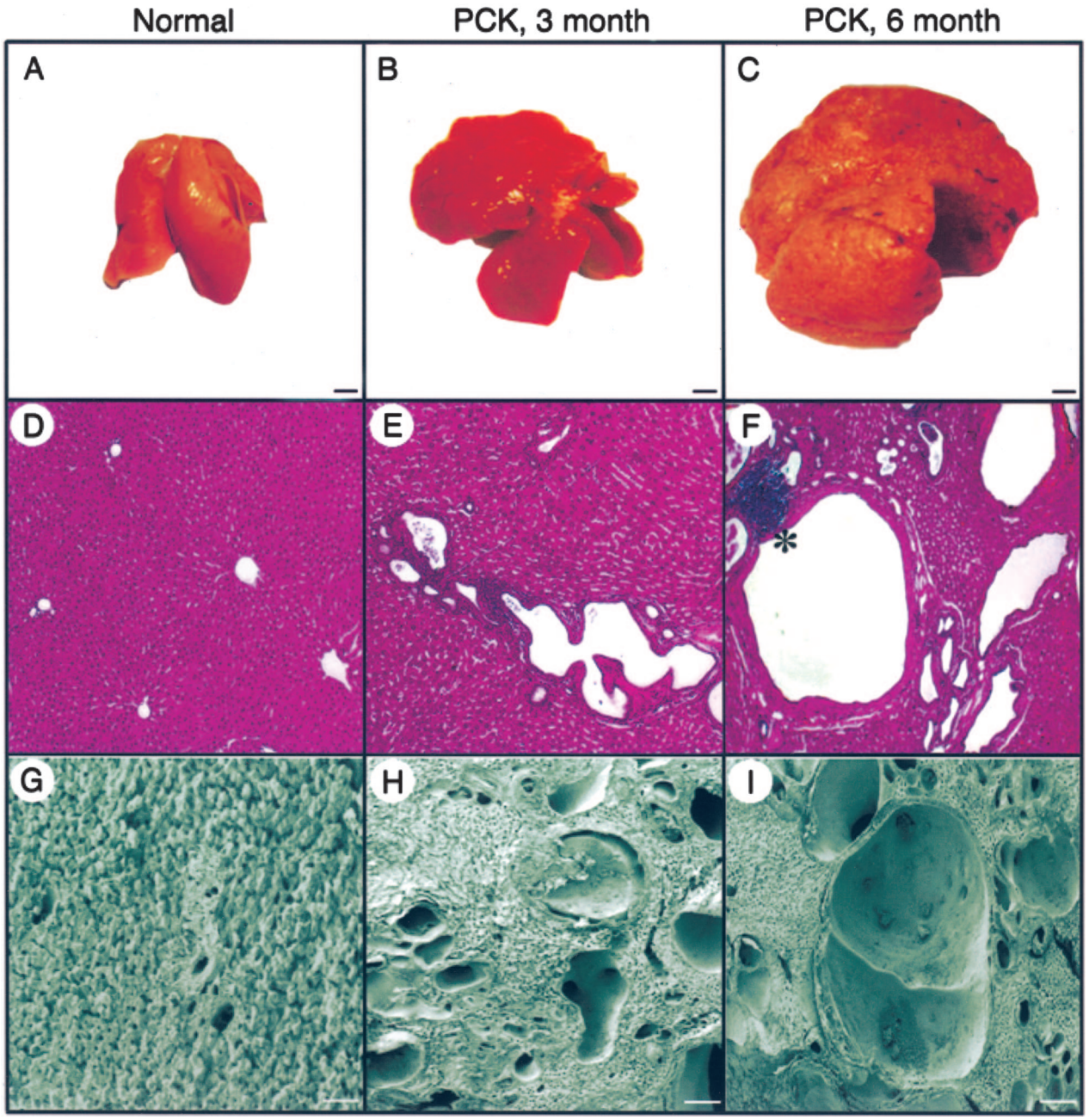

Figure 1. Gross anatomy and liver morphology in normal and PCK rats. **A–C:** At the gross level, livers in the PKC rats progressively enlarged with age. **D–F:** Light microscopy (H&E) and **G–I:** Scanning electron microscopy shows that some cysts are present in PCK rats at 3 month of age; by 6 months cysts replace most of the liver parenchyma. Portal inflammation was found occasionally in both groups of the PCK rats (**F**, **asterisk**). Scale bars: 5 mm (**A–C**); 200 μm (**G–I**). Original magnifications, $\times$40 (**D–F**).

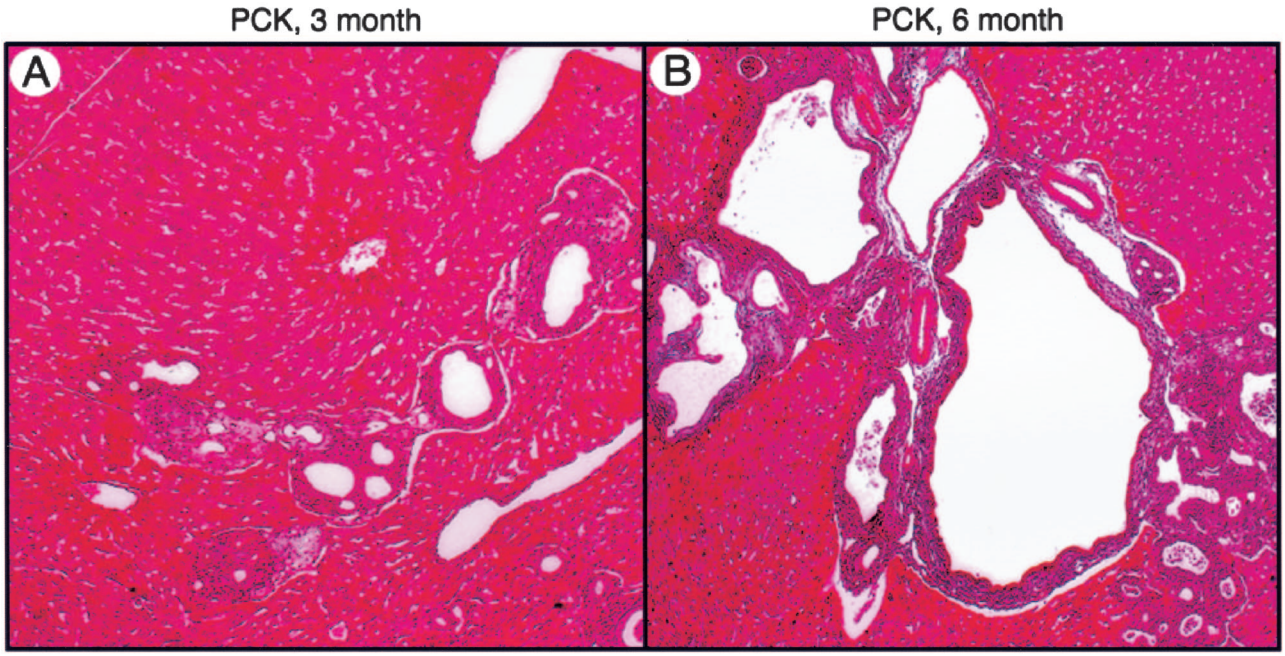

Figure 2. Representative images of the liver from 3-month-old (**A**) and 6-month-old (**B**) PCK rats stained with Masson's trichrome. Mild fibrosis without septa formation was found in 6-month-old PCK rats. Original magnifications, ×40.

crographs were used to measure the length of cilia in normal and PCK rats and the area of liver cysts in both groups of the PCK rats (ImageJ; NIH Images).

Statistical Analysis

All values were expressed as mean ± SEM. Ciliary length was expressed as mean ± SD. Statistical analysis was performed by the Student's *t*-test, and results were considered statistically different at $P < 0.05$.

Results

Gross Anatomy and Liver Pathology

Body weights were comparable in normal and PCK rats (data not shown). In contrast, PCK rats showed significant liver enlargement during disease progression (Figure 1; A to C). In 3- and 6-month-old normal rats, the liver (10.54 ± 1.53 g and 13.23 ± 2.18 g, respectively) represented ~4% of total body weight and this ratio remained unchanged throughout time.[38,39] In 3- and 6-month-old PCK rats, liver weights (23.61 ± 4.66 g and 41.57 ± 7.76 g, respectively) accounted for ~9% and 15% of total body weights. In both groups of PCK rats, the outer surface of the liver was diffusely deformed by numerous cysts that contained transparent or cloudy fluid varying in color from clear to yellow greenish.

Light (Figure 1; D to F) and scanning electron (Figure 1; G to I) microscopy showed that, with disease progression, cysts varied in size and shape and developed throughout the entire liver of PCK rats. In 3-month-old animals, the average area of liver cysts was 0.022 ± 0.01 mm^2 (range, 6.34 μm^2 to 0.75 mm^2). By 6 months, most of the liver parenchyma was replaced by cystic epithelia and the average area of cysts increased to 0.059 ± 0.02 mm^2 (range, 7.15 μm^2 to 1.12 mm^2). Cysts were surrounded by fibrous tissue in 3-month-old rats (Figure 2A) and a mild hepatic fibrosis without septa formation was observed in 6-month-old PCK rats (Figure 2B). Portal inflammations in both groups of PCK rats were rare (Figure 1F).

Morphology of the Liver Cysts

By microdissection (Figure 3, A and B) and scanning electron microscopy (Figure 3, C and D), we found that different types of cysts are present in the liver of PCK rats. Some cysts are single solitary cysts (Figure 3, A and C). The majority of cysts form lobulated structures (Figure 3, B and D). Cystic epithelia stained positively for the ductal epithelial cell marker, CK-19, suggesting that cysts originated from the biliary tree (Figure 3E). Ultrastructurally, cysts were lined by a single layer of normally differentiated cuboidal epithelial cells with well-formed microvilli and cell junctions (Figure 3F). Compared to normal cholangiocytes (Figure 3G), cystic cells were enlarged showing an increased number of mitochondria (23 ± 6 versus 7 ± 2 in normal rat, $P < 0.0001$) and flattening of the normally convoluted basement membrane.

Microscopic examination of the microdissected liver cysts (Figure 3A) showed that cysts were closed sacs with no openings and thus no connection to the biliary tree. Scanning electron microscopy of complementary hemispheres of a bisected liver cyst from a 6-month-old PCK rat (Figure 4) further supported the observation that liver cysts become isolated from the biliary tree.

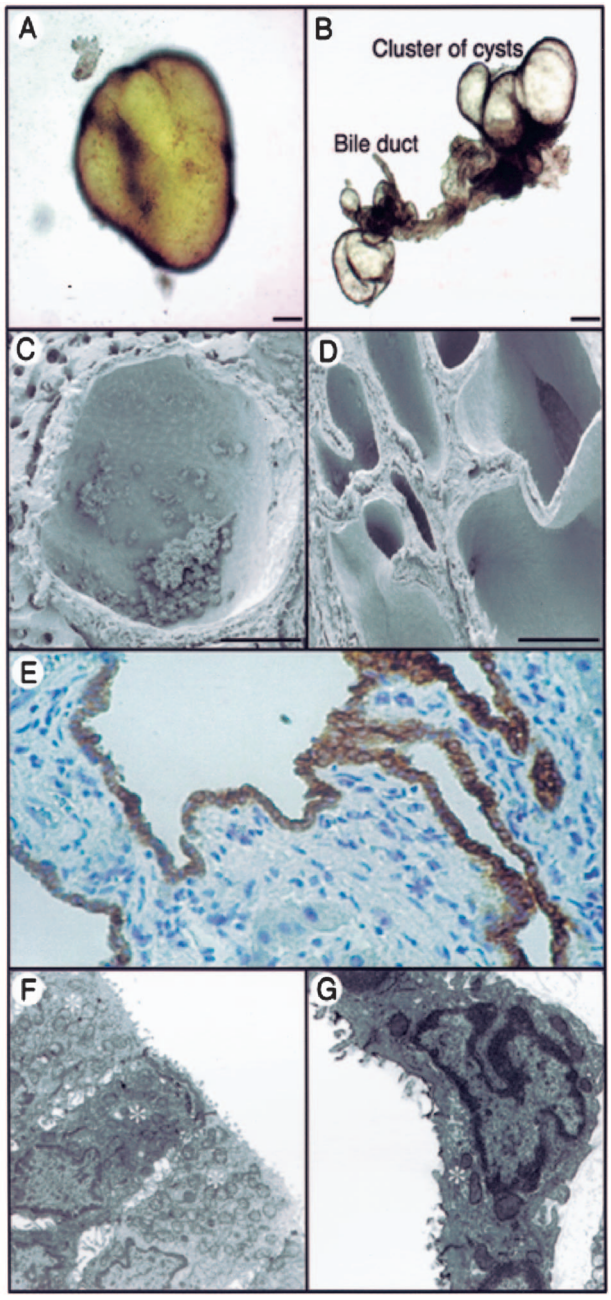

Figure 3. Morphology of the liver cyst. Single cyst (**A**) and cluster of cysts (**B**) isolated from the liver of the PCK rat by microdissection. **C** and **D:** Scanning electron microscopy of liver cysts. **E:** Cystic epithelia are positive for ductal epithelial cell marker, CK-19. Transmission electron microscopy of cells lining liver cysts in PCK rats (**F**) and bile duct in normal rats (**G**). **Asterisks** indicate mitochondria. Scale bars: 100 μm (**A**, **B**); 50 μm (**C**, **D**). Original magnifications: ×200 (**E**); ×6000 (**F**); ×15,000 (**G**).

Scanning (Figure 5, A and B) and transmission (Figure 5, D and E) electron microscopy showed that epithelial cells lining liver cysts possess primary cilia. Three hundred sixty-one cilia from 3-month-old (n = 3) and 418 cilia from 6-month-old (n = 3) PCK rats, and 198 cilia from normal rats (n = 5) were analyzed. In both groups of PCK rats, cilia were structurally abnormal with bulbous extensions of the ciliary tip or ciliary axonemal membrane (Figure 5), heterogeneous in length (range, 0.21 to 6.27 μm) and on average (3.35 ± 1.96 μm), significantly shorter then in normal cholangiocytes (6.63 ± 1.32 μm, $P < 0.0001$; Figure 5, C and F).

Three-Dimensional Reconstruction of the Biliary Tree

To reconstruct in three-dimension the biliary trees of normal and PCK rats under conditions that preserve the original morphology, we used a previously described technique involving micro-CT scanning and novel software. The representative reconstructed images of the intrahepatic biliary tree of the whole left lateral lobe of 3-month-old normal and PCK rats are shown in Figure 6, A and B, respectively. In 6-month-old PCK rats the left lateral lobe was cut into distal, middle, and proximal (Figure 6C) parts because of size limitation of the micro-CT-scanned specimens.

The biliary tree in PCK rats undergoes sequential and significant remodeling, resulting in multiple segmental and saccular dilatations and focal buddings. Quantitative analysis of the pathological changes in biliary tree architecture in the PCK rat is shown in Table 1. Diameters of the proximal bile ducts in 3- and 6-month-old PCK rats were 3 and 5 times larger, respectively, than in normal rats. The distal bile ducts were also dilated in the PCK rat. The diameters of bile duct segments in normal rats consistently decreased along the biliary tree axis. However, in the PCK rat, bile ducts with large and small diameters occurred at each level of the biliary tree. In normal rats, the biliary tree is composed of approximately nine bile duct interbranch segments with an average length of 1.4 mm. In 3-month-old PCK rats, the number of bile duct interbranch segments increased up to 15 with an average length 1.82 mm and these parameters did not change significantly by 6 months.

In 3-month-old PCK rats, the total volume of the intrahepatic biliary tree (892 ± 229 μl) was 19-times greater ($P < 0001$) than in normal rats (47 ± 7 μl). Such dramatic volume enlargement reflects bile duct dilatation and massive formation of cysts that are attached to the biliary tree (Figure 6B, inset). As clearly demonstrated by the reconstructed images (Figure 6C, insets), in 6-month-old PCK rats many cysts were disconnected from the bile ducts resulting in decreased biliary tree volume (484 ± 108 μl) compared to 3-month-old rats.

The intrahepatic biliary trees of normal and PCK rats shown in Figure 6 were scanned at a resolution of 20 μm; thus, bile ducts less than 20 μm in diameter were below the scanning resolution. To visualize the small bile ducts, we also scanned small pieces of liver lobes (close to the edge) from normal and PCK rats (data not shown) with a resolution of 5 μm. We found in the PCK rats the same pattern of changes (ie, bile duct dilatation and clusters of cysts) such as we had seen in the biliary tree scanned with a resolution of 20 μm. The data suggest that cystogenesis affects all segments of the biliary tree.

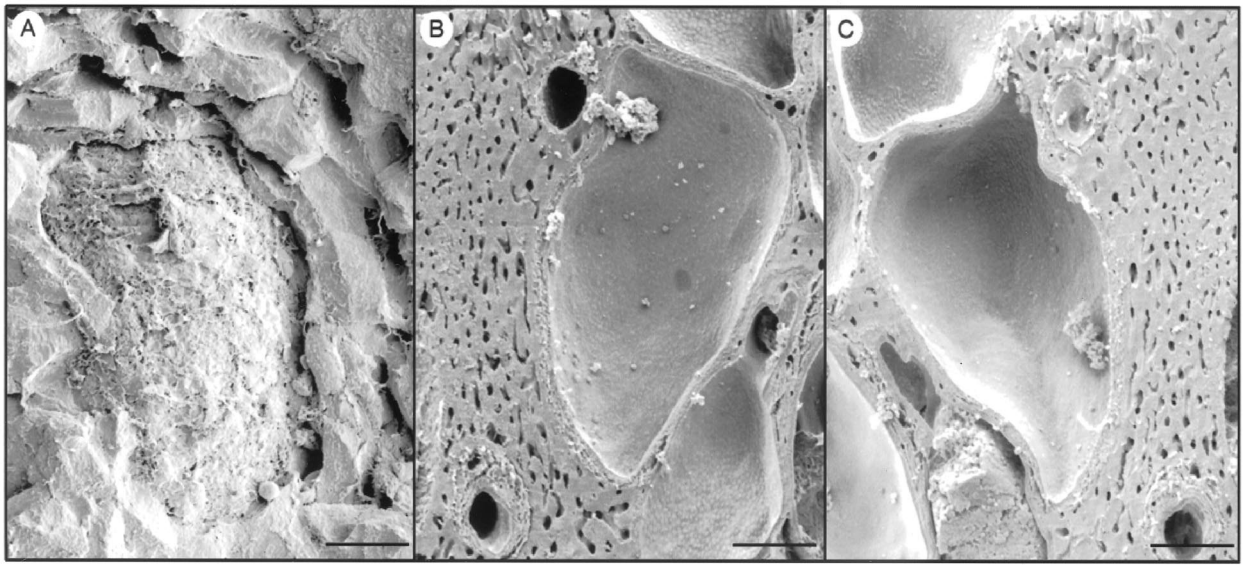

Figure 4. Scanning electron microscopy of bisected liver cyst from 6-month-old PCK rats. **A:** Single liver cyst embedded in liver parenchyma. **B** and **C:** Complementary hemispheres of the bisected liver cyst showed that cyst has no openings and thus, no connections to the bile duct. Scale bars: 20 μm (**A**); 200 μm (**B**, **C**).

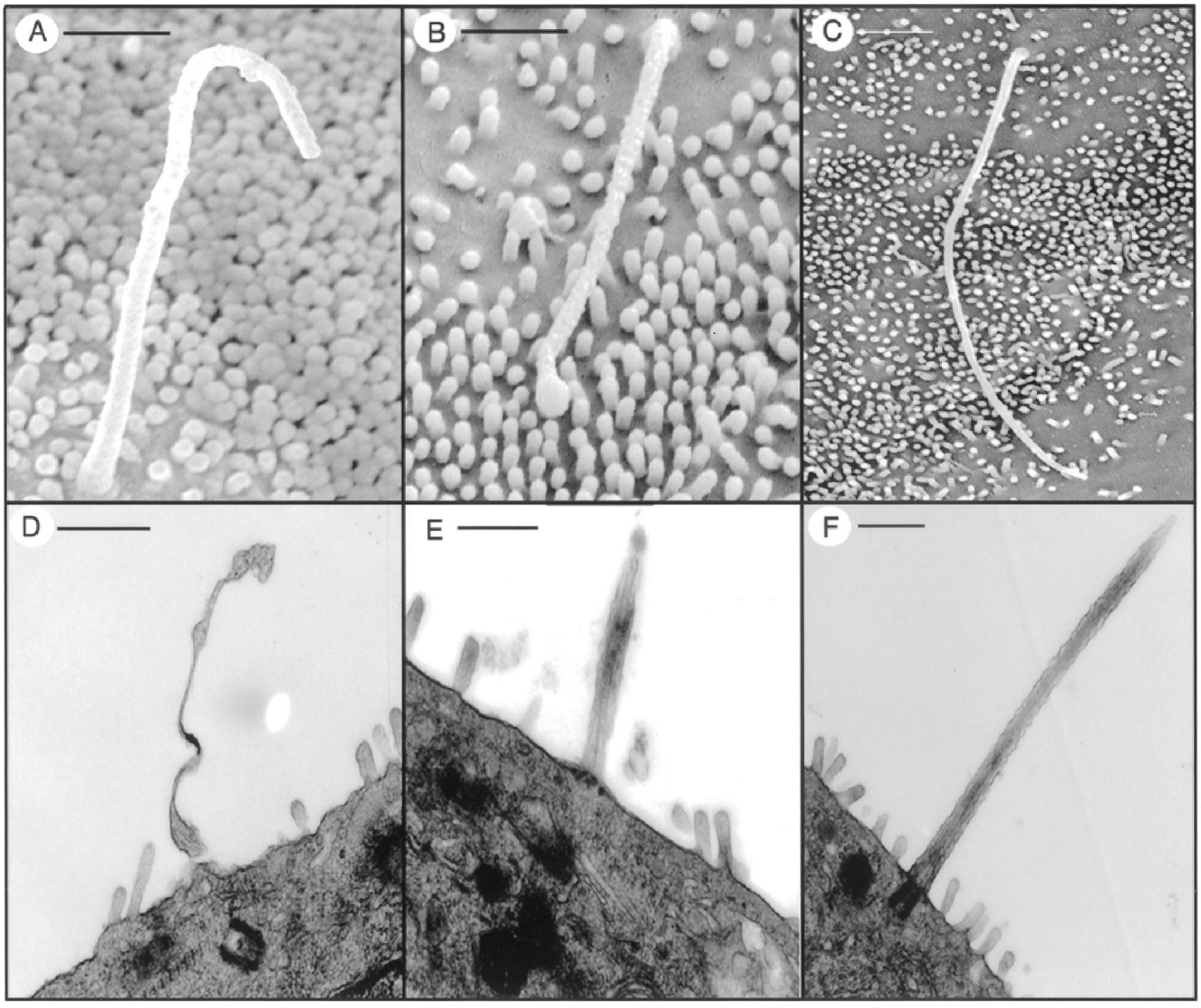

Figure 5. The diversity in ciliary length and the structural abnormalities in the PCK rat by scanning (**top**) and transmission (**bottom**) electron microscopy. **A** and **B:** Cilia from cystic epithelial cells are variable in length compared to cilia of normal cholangiocytes (**C**). **D** and **E:** Malformed cilia with bulbous extension of the axonemal membrane were seen in the PCK rat but not in normal rat (**F**). Scale bars: 500 nm (**A**, **B**); 1 μm (**C–F**).

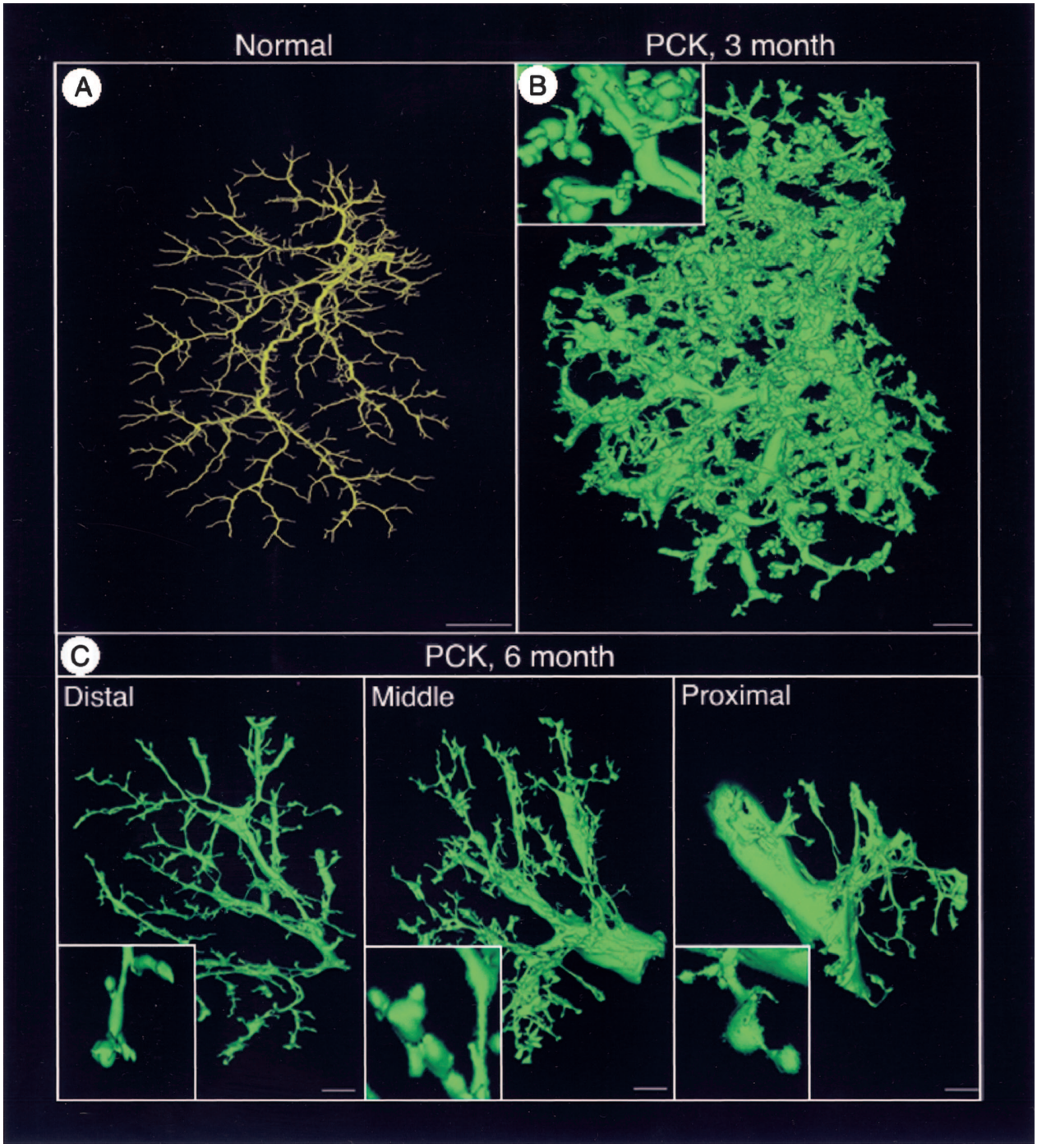

Figure 6. The brightest voxel projection of the intrahepatic biliary tree scanned with resolutions of 20 μm of the left lateral lobe from 3-month-old normal (**A**) and 3-month-old (**B**) and 6-month-old (**C**) PCK rats. The liver lobe in 6-month-old PCK rat was cut into three parts: distal, middle, and proximal. **Insets** in **B** and **C** show a high-magnification image. Scale bars: 2 mm (**A**); 1 mm (**B**, **C**).

Quantitation of Total Parenchymal and Total Cystic Volume in the PCK Rat

To measure total liver, parenchymal, and cystic volumes, intact liver lobes from 3-month-old (Figure 7A) and 6-month-old (representative image not shown) normal rats; and 3-month-old (Figure 7B) and 6-month-old (Figure 7C) PCK rats were scanned and reconstructed in three-dimensions. Liver parenchyma (white) and cysts (black spots) were easily defined on CT images. The total liver volume was assumed to consist of only parenchyma and cysts. Total liver and total cystic volume was measured, and total parenchymal volume calculated as a difference between these two.

Table 1. Quantitative Analysis of the Intrahepatic Biliary Tree in Normal and Two Groups of PCK Rats by Three-Dimensional Reconstruction

	Normal rat	PCK rat	
		3 month old	6 month old
Diameter (μm)			
Proximal segments	218 ± (38)	596 ± (198)*	1078 ± (265)*†
Distal segments	21 ± (6)	37 ± (7)*	39 ± (67)*
Number of interbranch segments	9 ± (3)	15 ± (6)*	16 ± (4)*
Length of interbranch segment (mm)	1.44 ± (0.39)	1.82 ± (0.32)*	2.15 ± (0.49)*
Length of the biliary tree (mm)	14.48 ± (4.94)	25.17 ± (7.65)*	26.64 ± (8.39)*
Biliary tree volume (μl)	47 ± (7)	892 ± (229)*	484 ± (108)*†

*Compare to normal rats.
†Compare to 3-month-old PCK rats; $P < 0.05$.

In normal rats, liver volume is equal to parenchymal volume. Results of the quantitative analysis are shown in Table 2. In both groups of PCK rats, total liver volume was significantly increased compared to age-matched normal rats. However, parenchymal volume in the PCK rats was not altered by liver cysts and was similar to that in normal rats. Total cystic volume was age-dependent. In 3-month-old (9 ± 2 ml) and 6-month-old (28 ± 7 ml) PCK rats it represented 40.5% and 68.3%, respectively, of total liver volume.

We found a strong correlation between total liver volume and total cystic volume (Figure 8) but not parenchymal volume. In addition, the intercept at a cyst volume of 0 ml was ~13 ml, identical to the hepatic parenchymal volume of normal rats. To assess if the preserved hepatic volume in the PCK rats is associated with normal liver function, serum levels of aspartate aminotransferase, alanine aminotransferase, alkaline phosphatase, albumin, total protein, and bilirubin were measured (Table 3). Hepatic function tests were not different between normal and PCK rats at the age of 3 months. In 6-month-old PCK rats, the levels of aspartate and alanine aminotransferases were increased compared to age-matched controls.

Liver Cysts Are Disconnected from the Biliary Tree

In Figure 9, single micro-CT slices (21 μm in thickness) of a liver lobe from normal (Figure 9A) and 3-month-old (Figure 9B) and 6-month-old PCK rats (Figure 9C) are shown. White dots on the gray liver surface of the normal and PCK rats represent the cross-sections of the intrahepatic bile ducts filled with the contrast agent, which we use for biliary tree visualization. In contrast to 3-month-old PCK rats, in which only the parenchyma (gray) and dilated bile ducts (white spots) were observed, in 6-month-old PCK rats liver cysts (black spots and asterisks) were easily defined by micro-CT images. It is clear that these cysts do not fill with contrast agent suggesting that, at this

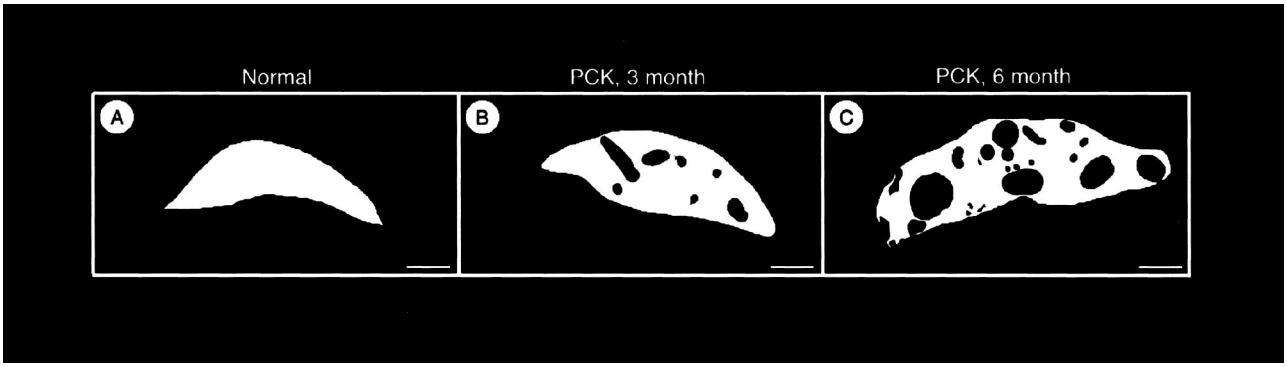

Figure 7. Micro-CT images of the intact liver lobes of normal (**A**) and 3-month-old (**B**) and 6-month-old (**C**) PCK rats reconstructed in three-dimension. These images were used to measure total liver, parenchymal, and cystic volumes. Scale bars, 2 mm.

Table 2. Quantitation of Total Liver, Parenchymal, and Cystic Volumes in Two Aged Groups of Normal and PCK Rats

	Normal rats		PCK rats	
Total volume, (ml)	3 month	6 month	3 month	6 month
Liver	13 ± 2	15 ± 2	21 ± 5*	41 ± 7*†
Parenchyma	13 ± 2	15 ± 2	13 ± 3	13 ± 4
Cysts	0	0	9 ± 2	28 ± 7†

*Compared to normal rats.
†Compare to 3-month-old PCK rats; $P < 0.05$.
Total liver volume in normal rats is equal to parenchymal volume.

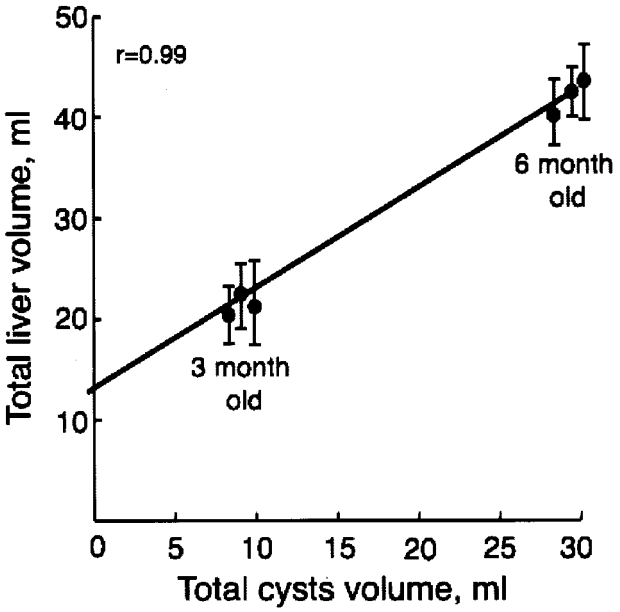

Figure 8. Relationship between total liver and total cystic volume in 3- and 6-month-old PCK rats shows that cyst volume correlates strongly with total liver volume.

stage of cystogenesis, they do not communicate with the biliary tree.

Discussion

This study relates to the liver phenotype of the PCK rat, a useful animal model of ARPKD. Our major findings are: 1) at 3 months, the majority of cysts are connected to the biliary tree and by 6 months, most cysts are disconnected from the bile ducts; 2) the liver progressively enlarged because of massive cyst formation while hepatic parenchymal volume is preserved; 3) the intrahepatic biliary tree undergoes extensive remodeling resulting in dilatation of the bile ducts, focal budding, and formation of cysts; 4) cysts originate from all bile duct segments along the biliary tree axis; and 5) in epithelial cells lining liver cysts primary cilia are malformed and shortened. These findings not only provide additional guidance for the utility of the PCK rat for studying ARPKD but also give important clues as to the pathogenesis and progression of ARPKD.

The present study used a variety of techniques to describe the biliary phenotype in the PCK at two different time points of disease development to understand liver pathology that is a major cause of death in older ARPKD patients. Our microscopic data showing age-dependent progression of cystic lesions in the liver of the PCK rat are consistent with previously made observations.[22,23]

To assess that liver enlargement in the PCK rats is the result of massive cyst formation but does not involve changes in liver parenchyma, we reconstructed in three-dimensions intact liver lobes from normal and PCK rats. Computed tomographic methods to measure cystic volume in plastic agar models (in this model plastic cysts were embedded in agar) and in patients with ADPKD (without intravenous injection of contrast) had shown that this method is valid and accurate.[41,42] Our published data[43] also suggest that micro-CT images could be used to precisely measure the total liver tissue volume. In the PCK rat, liver parenchyma and cysts (based on differences in their densities) were easily defined by micro-CT images. Quantitation analysis clearly showed that the major determinant of progressive liver enlargement in the PCK rats is a massive cyst formation. Parenchymal volume was constant and preserved during the disease progression. Hepatic function tests were normal in 3-month-old PCK rats whereas elevations in serum levels of aspartate and alanine aminotransferases were found in 6-month-old PCK rats. These data are in agreement with previously made observations that, in the PCK rat, some laboratory parameters increase with disease progression.[23]

Isolation of the hepatic and renal cysts from the biliary tree and kidney tubules, respectively, during disease progression is well characterized in ADPKD.[5,37] To our knowledge, no information is available on the progression of kidney or liver cysts throughout time in ARPKD. Experimental data presented here strongly suggest that in the PCK rat, cysts disconnect from the biliary tree with advancing age. First, scanning electron microscopy of bisected hemispheres of the liver cysts showed no openings and thus no connections to the bile duct. Second, cysts isolated from the liver by microdissection were closed sacs. Third, three-dimensional images of liver slices from PCK rats showed that cysts (in contrast to bile ducts) did not fill with contrast agent used to visualize the intrahepatic biliary tree. Fourth, three-dimensional images of the intrahepatic biliary tree in 3-month-old PCK rats showed that the majority of cysts were still connected

Table 3. Liver Function Test in Normal and PCK Rats

	3 month old		6 month old	
	Normal	PCK	Normal	PCK
Aspartate amino transferase (U/L)	110 ± (24)	112 ± (14)	92.50 ± (10)	225 ± (36)*†
Alkaline phosphatase (U/L)	139 ± (10)	150 ± (11)	126 ± (11)	170 ± (19)*
Alanine amino transferase (U/L)	72 ± (5)	76 ± (2)	88 ± (12)	74 ± (4)
Albumin (g/dL)	4.0 ± (0.05)	3.9 ± (0.17)	4.2 ± (0.26)	3.6 ± (0.38)
Total protein (g/dL)	6.0 ± (0.09)	5.7 ± (0.06)	6.2 ± (0.32)	6.2 ± (0.07)
Bilirubin (mg/dL)	0.20 ± (0.04)	0.23 ± (0.03)	0.18 ± (0.03)	0.26 ± (0.06)

*Compare to normal rats.
†Compare to 3-month-old PCK rats; $P < 0.05$.

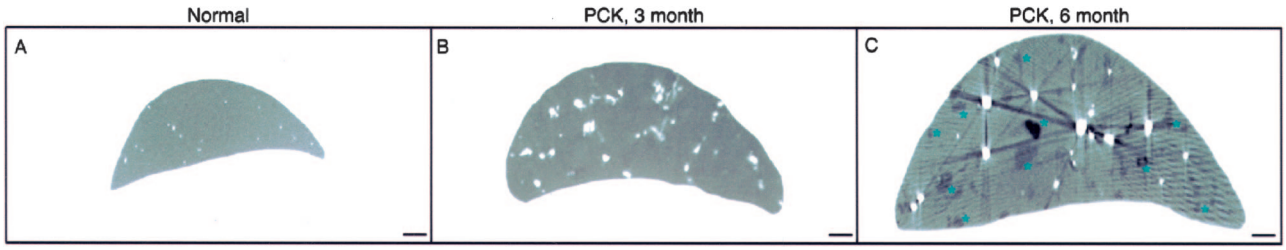

Figure 9. Micro-CT images of the single liver slice (21 μm) of 3-month-old normal (**A**) and 3-month-old (**B**) and 6-month-old (**C**) PCK rats. **White dots** represent cross-sections of the bile ducts filled with contrast agent. **Black spots** are liver cysts. Note that cysts do not fill with contrast agent suggesting that they are disconnected from the biliary tree. **Asterisks** indicate liver cysts that do not fill with contrast agent. Scale bars, 2 mm.

to the bile ducts accounting for the dramatic increase of the biliary tree volume (892 ± 229 μl) compared to control (47 ± 7 μl). By the age of 6 months, however, the majority of cysts separated from the bile ducts, and, as a result, biliary tree volume decreased compared to 3-month-old PCK rats (484 ± 108 μl). To begin to understand the mechanisms of cyst separation from the biliary tree in the PCK rat, we analyzed micro-CT-scanned liver slices or fully reconstructed intrahepatic biliary trees. Serial liver slices or reconstructed biliary tree were displayed at different angles of view to better understand the relationships between cyst and bile duct. Many cysts were attached to the biliary tree (Figure 6B) whereas others appeared to lose their connection with bile ducts (Figure 6C, proximal part, inset) suggesting that cysts pinch off from the biliary tree. However, additional studies are needed to understand this process. Although the mechanisms of cyst formation and separation from the biliary tree in autosomal recessive PKD are still unknown, our data clearly demonstrate that, with age in the PCK rat, cysts become separated from the bile duct.

Ultrastructurally, epithelial cells lining liver cysts were enlarged with increased numbers of mitochondria. It has been suggested that an increase in mitochondrial quantity relates to cell energy demands and reflects an increased level of metabolic activity. An increased number of mitochondria have been documented in a wide variety of cells during transitions from normal to pathological or disease states.[44,45]

In both groups of the PCK rats, we found that cilia were shortened and aberrantly structured. Recent studies have indicated that various forms of PKD are associated with structural and/or functional abnormalities of primary cilia, suggesting a causative role for this organelle in disease development. For example, in ARPDK mouse models, *orpk*, *cpk*, *and inv* their respective protein products (polaris,[32,33,46] cystin,[31,33] and inversin[30,47]) are localized to primary cilia. Defects in polaris expression result in short stunted cilia in the kidney, retina, and embryonic node. Additional evidence for a role of primary cilia in the pathogenesis of PKD is derived from kidney-specific *Kif3a* knockout mice. Disruption of *Kif3a* (a motor subunit of kinesin II that moves particles along ciliary microtubules and is critically important in assembly and maintenance of ciliary structure and function) results in complete absence of cilia in kidney epithelial cells and cyst formation from mature renal tubules.[48]

Our previously published data[27] suggest that, under normal conditions, fibrocystin is expressed in primary cilia of cholangiocytes. In the PCK rat, a splicing mutation of *Pkhd1* results in structural and functional ciliary abnormalities. Based on fibrocystin homology to several known proteins such as plexins and HGF-met,[24,26] it has been proposed that fibrocystin is a receptor protein involved in

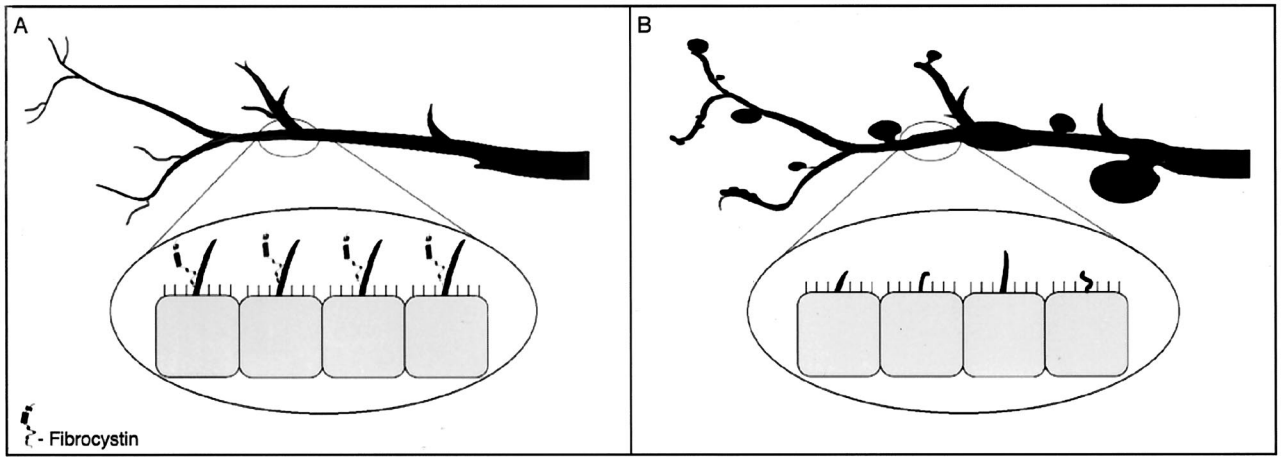

Figure 10. Model of fibrocystin-dependent terminal differentiation of the biliary tee. **A:** In normal rats, fibrocystin is localized to cholangiocyte cilia and functions as a bile duct size sensor controlling maturation of the biliary tree. **B:** In PCK rats, cilia are shortened, malformed, and do not express fibrocystin leading to abnormalities in cell proliferation and differentiation, ultimately resulting in significant bile duct dilatation and cyst formation.

terminal differentiation of collecting ducts in kidney and bile ducts in liver. Thus in normal rats, fibrocystin may function as a bile duct size sensor controlling maturation of the biliary tree (Figure 10A). In PCK rats, structural (cilia are shortened and malformed) and functional (fibrocystin is not express in cilia) defects in cholangiocyte cilia may lead to abnormalities in cell proliferation and biliary tree differentiation, ultimately resulting in significant bile duct dilatation and cyst formation (Figure 10B). Finally, a possible role for cilia and ADPKD-related proteins, polycystin-1 and polycystin-2, in control of kidney tubule size has been suggested.[49]

In conclusion, the PCK rat has several features that resemble human ARPKD. As in the human, polycystic disease in the PCK rat is inherited in an autosomal recessive manner and severity of liver cystic lesions is age-dependent. Results of our study strongly suggest that the PCK rat will be useful for studies of biliary cystogenesis and possible treatment approaches to inherited cystic liver disease.

References

1. Iglesias DM, Palmitano J, Arrizurieta E, Kornblihtt AR, Herrera M, Bernath V, Matrin RS: Isolated polycystic liver disease not linked to polycystic kidney disease 1 and 2. Dig Dis Sci 1999, 44:385–388
2. Pirson Y, Lannoy N, Peters D, Guubel A, Gigot J-F, Breuning M, Verellen-Dumoulin C: Isolated polycystic liver disease as a distinct genetic disease, unlinked to polycystic kidney disease 1 and polycystic kidney disease 2. Hepatology 1996, 23:249–252
3. Li A, Davila S, Furu L, Qian Q, Tian X, Kamath PS, King BF, Torres VE, Somlo S: Mutations in PRKCSH cause isolated autosomal dominant polycystic liver disease. Am J Hum Genet 2003, 72:691–703
4. Drenth JPH, teMorsche RHM, Smink R, Bonifacino JS, Jansen JBMJ: Germline mutations in PRKCSH are associated with autosomal dominant polycystic liver disease. Nat Genet 2003, 33:345–347
5. Calvet JP, Grantham JJ: The genetic and physiology of polycystic kidney disease. Semin Nephrol 2001, 21:107–123
6. Guay-Woodford LM: Autosomal Recessive Polycystic Kidney Disease: Clinical and Genetic Profiles. Edited by ML Watson. New York, Oxford University Press, 1996, pp 237–266
7. Zerres K, Mucher G, Becker J, Steinkamm C, Rudnik-Schoneborn S, Heikkila P, Rapola J, Salonen R, Germino GG, Onuchic L, Somlo S, Avner ED, Harman LA, Stockwin JM, Guay-Woodord LM: Prenatal diagnosis of autosomal recessive polycystic kidney disease: molecular genetics, clinical experience, and fetal morphology. Am J Med Genet 1998, 76:137–144
8. Wilson PD: Polycystic kidney disease. N Engl J Med 2004, 350:151–164
9. Gretz N, Hocker A, Baur S, Lasserre JJ, Bachmann S, Waldherr R, Strauch M: Rat Models of Polycystic Kidney Disease. Edited by MH Breuning, M Devoto, G Romeo. Basel, Karger, 1992, pp 35–46
10. McDonald RA, Avner ED: Mouse Models of Polycystic Kidney Disease. Edited by ML Watson. New York, Oxford University Press, 1996, pp 63–87
11. Schieren G, Pey R, Bach J, Hafner M, Gretz N: Murine models of polycystic kidney disease. Nephrol Dial Transplant 1996, 11:38–45
12. Guay-Woodford LM: Murine models of polycystic kidney disease: molecular and therapeutic insights. Am J Physiol 2003, 285:F1034–F1049
13. Fry J, Koch W, Jennette J, McFarland E, Fried F, Mandell J: A genetically determined murine model of infantile polycystic kidney disease. J Urol 1985, 134:828–833
14. Moyer JH, Lee-Tischler MJ, Kwon H-Y, Schrick JJ, Awner ED, Sweeney WE, Godfrey VL, Cacheiro NLA, Woychik RP, Wilkinson JE: Candidate gene associated with a mutation causing recessive polycystic kidney disease in mice. Science 1999, 264:1329–1333
15. Ricker JL, Gattone II VH, Calvet JP, Rankin CA: Development of autosomal recessive polycystic kidney disease in BALB/c-cpk/cpk mice. J Am Soc Nephrol 2000, 11:1837–1847
16. Chittenden L, Lu X, Cacheiro NLA, Cain KT, Geneeroso W, Bryda E, Stubb L: A new mouse model for autosomal recessive polycystic kidney disease. Genomics 2002, 79:499–504
17. Gattone VH, MacNaughton KA, Kraybill AL: Murine autosomal recessive polycystic kidney disease with multiorgan involvement induced by cpk gene. Anat Rec 1996, 245:488–499
18. Guay-Woodford L, Green W, Lindsey J, Beier D: Germline and somatic loss-of-function of the mouse cpk gene causes biliary ductal pathology that is genetically modulated. Hum Mol Genet 2000, 9:769–778
19. Nauta J, Ozawa Y, Sweeney Jr WE, Rutledge JC, Avner ED: Renal and biliary abnormalities in a new murine model of autosomal recessive polycystic kidney disease. Pediatr Nephrol 1993, 7:163–172
20. Grimm PC, Crocker JFS, Malatjalian DA, Ogborm MR: The microanatomy of the intrahepatic bile duct in polycystic disease: comparison of the cpk mouse and human. J Exp Pathol 1990, 71:119–131
21. Katsuyama M, Masuyama T, Komura I, Hibino T, Takahashi H: Characterization of a novel polycystic kidney rat model with accompanying polycystic liver. Exp Anim 2000, 49:51–55
22. Sanzen T, Harada K, Yasoshima M, Kawamura Y, Ishibashi M, Nakanuma Y: Polycystic kidney rat is a novel animal model of Caroli's disease associated with congenital hepatic fibrosis. Am J Pathol 2001, 158:1605–1612
23. Lager DJ, Qian Q, Bengal RJ, Ishibashi M, Torres VE: The PCK rat: a new model that resembles human autosomal dominant polycystic kidney and liver disease. Kidney Int 2001, 59:126–136
24. Ward CJ, Hogan MC, Rossetti S, Walker D, Sneddon T, Wang X, Kubly V, Cunningham JM, Bacallao R, Ishibashi M, Milliner DS, Torres VE, Harris PC: The gene mutated in autosomal recessive polycystic kidney disease encodes a large, receptor-like protein. Nat Genet 2002, 30:259–269
25. Bergmann C, Senderek J, Sedlacek B, Pegiazoglou I, Puglia P, Eggermann T, Rudnik-Schneborn S, Furu L, Onuchic LF, DeBaca M, Germino GG, Guay-Woodford L, Somlo S, Moser M, Buttner R, Zerres K: Spectrum of mutations in the gene for autosomal recessive polycystic kidney disease (ARPKD/PKHD1). J Am Soc Nephrol 2003, 14:76–89
26. Onuchic LF, Furu L, Nagasawa Y, Hou X, Eggermann T, Ren Z, Bergmann C, Senderek J, Esquivel E, Zeltner R, Rudnik-Schoneborn S, Mrug M, Sweeney W, Avner ED, Zerres K, Guay-Woodford LM, Somlo S, Germino GG: PKHD1, the polycystic kidney and hepatic disease 1 gene, encodes a novel large protein containing multiple immunoglobulin-like plexin-transcription-factor domains and parallel beta-helix 1 repeats. Am J Hum Genet 2002, 70:1305–1317
27. Masyuk TV, Huang BQ, Ward CJ, Masyuk AI, Yuan D, Splinter PL, Punyashthiti R, Ritman EL, Torres VE, Harris PC, LaRusso NF: Defects in cholangiocyte fibrocystin expression and ciliary structure in the PCK rat. Gastroenterology 2003, 125:1303–1310
28. Ward CJ, Yuan D, Masyuk T, Wang X, Punyashthiti R, Whelan S, Bacallao R, Torra R, LaRusso NF, Torres VE, Harris PC: Cellular and subcellular localization of the ARPKD protein; fibrocystin is expressed on primary cilia. Hum Mol Genet 2003, 15:2703–2710
29. Pazour GJ, Dickert BL, Vucica Y, Seeley ES, Rosenbaum JL, Witman GB, Cole DG: Chlamydomonas IFT88 and its mouse homologue, polycystic kidney disease gene tg737, are required for assembly of cilia and flagella. J Cell Biol 2000, 151:709–718
30. Watanabe D, Saijoh Y, Nonaka S, Sasaki G, Ikawa Y, Yokoyama T, Hamada H: The left-right determinant Inversin is a component of node monocilia and other 9+0 cilia. Development 2003, 130:1725–1734
31. Hou X, Mrug M, Yoder BK, Lefkowitz EJ, Kremmidiotis G, D'Eustachio PD, Beier DR, Guay-Woodford LM: Cystin, a novel cilia-associated protein, is disrupted in the cpk mouse model of polycystic kidney disease. J Clin Invest 2002, 109:533–540
32. Taulman PD, Haycraft CJ, Balkovetz DF, Yoder BK: Polaris, a protein involved in left-right axis patterning, localizes to basal bodies and cilia. Mol Biol Cell 2002, 12:589–599
33. Yoder BK, Hou X, Guay-Woodford LM: The polycystic kidney disease proteins, polycystin-1, polycystin-2, polaris, and cystin, are co-localized in renal cilia. J Am Soc Nephrol 2002, 13:2508–2516
34. Pazour GJ, San Agustin JT, Follit JA, Rosenbaum JL, Witman GB: Polycystin-2 localizes to kidney cilia and the ciliary level is elevated in

orpk mice with polycystic kidney disease. Curr Biol 2002, 12:R378–R380
35. Wang S, Luo Y, Wilson PD, Witman GB, Zhou J: The autosomal recessive polycystic kidney disease protein is localized to primary cilia, with concentration in the basal body area. J Am Soc Nephrol 2004, 15:592–602
36. Zhang MZ, Mai W, Li C, Cho SY, Hao C, Moeckel G, Zhao R, Kim I, Wang J, Xiong H, Wang H, Sato Y, Wu Y, Nakanuma Y, Lilova M, Pei Y, Harris RC, Li S, Coffey RJ, Sun L, Wu D, Chen XZ, Breyer MD, Zhao ZJ, McKanna JA, Wu G: PKHD1 protein encoded by the gene for autosomal recessive polycystic kidney disease associates with basal bodies and primary cilia in renal epithelial cells. Proc Natl Acad Sci USA 2004, 101:2311–2316
37. Patterson M, Gonzalez-Vitale JC, Fagan CJ: Polycystic liver disease: a study of cyst fluid constituents. Hepatology 1982, 2:475–478
38. Vollmar B, Pradarutti S, Richter S, Menger MD: In vivo quantification of ageing changes in the rat liver from early juvenile to senescent life. Liver 2002, 22:330–341
39. Hall DM, Oberley TD, Moseley PM, Buettner GR, Oberley LW, Weindruch R, Kregel KC: Caloric restriction improves thermotolerance and reduces hyperthermia-induced cellular damage in old rats. FASEB J 2000, 14:78–86
40. Masyuk TV, Ritman EL, LaRusso NF: Quantitative assessment of the rat intrahepatic biliary system by three-dimensional reconstruction. Am J Pathol 2001, 158:2079–2088
41. Everson GT, Scherzinger A, Berger-Leff N, Reichen J, Lezotte D, Mango-Johnson M, Gabow P: Polycystic liver disease: quantitation of parenchymal and cystic volumes from computed tomography images and clinical correlates of hepatic cysts. Hepatology 1988, 8:1627–1634
42. King BF, Reed JE, Berkgstralh EJ, Sheedy II PF, Torres VE: Quantitation and longitudinal trends of kidney, renal cysts, and renal parenchyma volumes in autosomal dominant polycystic kidney disease. J Am Soc Nephrol 2000, 11:1505–1511
43. Masyuk TV, Ritman EL, LaRusso NF: Hepatic artery and portal vein remodeling in rat liver: vascular response to selective cholangiocyte proliferation. Am J Pathol 2003, 162:1175–1182
44. Perkins GA, Ellisman MH, Fox DA: Three-dimensional analysis of mouse rod and cone mitochondrial cristae architecture: bioenergetic and functional implications. Mol Vis 2003, 9:60–73
45. Szewczyk A, Wojtczak L: Mitochondria as a pharmacological target. Pharmacol Rev 2002, 54:101–127
46. Yoder BK, Tousson A, Millican L, Wu JH, Bugg Jr CE, Schafer JA, Balkovetz DF: Polaris, a protein disrupted in orpk mutant mice, is required for assembly of renal cilium. Am J Physiol 2002, 282:F541–FF552
47. Otto EA, Schermer B, Obara T, O'Toole JF, Hiller KS, Mueller AM, Ruf RG, Hoefele J, Beekmann F, Landau D, Foreman JW, Goodship JA, Strachan T, Kispert A, Wolf MT, Gagnadoux MF, Nivet H, Antignac C, Walz G, Drummond IA, Benzing T, Hildebrandt F: Mutations in INVS encoding inversin cause nephronophthisis type 2, linking renal cystic disease to the function of primary cilia and left-right axis determination. Nat Genet 2003, 34:413–420
48. Lin F, Hiesberger T, Cordes K, Sinclair AM, Goldstein LSB, Somlo S, Igarachi P: Kidney-specific inactivation of the KIF3A subunit of kinesis-II inhibits renal ciliogenesis and produces polycystic kidney disease. Proc Natl Acad Sci USA 2003, 100:5286–5291
49. Lubarsky B, Krasnow MA: Tube morphogenesis: making and shaping biological tubes. Cell 2003, 112:19–28